ACS OMEGA

Open Access

http://pubs.acs.org/journal/acsodf

Article

Stability of Cesium-Based Lead Halide Perovskites under UV Radiation

Zhiyang Qin, Jesus Alfonso Caraveo-Frescas, Leunam Fernandez-Izquierdo, M. Josefina Arellano-Jimenez, Francisco S. Aguirre-Tostado, Martin Gregorio Reyes-Banda, and Manuel A. Quevedo-Lopez*

Cite This: *ACS Omega* 2024, 9, 26683−26691

Read Online

ACCESS | Metrics & More | Article Recommendations | Supporting Information

ABSTRACT: Lead halide perovskites have been extensively studied for their potential applications, including photodetectors, solar cells, and high-energy radiation detection. These applications are possible because of their unique optoelectronic properties, such as tunable band gap, high optical absorption coefficient, and unique defect self-healing properties, which result in high defect tolerance. Despite these advantages, the long-term stability remains a critical issue that could hinder commercial applications of these materials. Reports on the stability of lead halide perovskites for optoelectronic applications have normally focused on methylammonium (MA)/formamidinium (FA), with very limited information for other systems, in particular, Cs-containing perovskites. In this paper, we report the stability of thick $CsPbBr_{3-x}Cl_x$ polycrystalline thin films (~8 μm) with several halide Br−Cl ratios after exposure to deep UV radiation. The chemical, crystal structure, optical, and electrical properties are analyzed, and the results are used to propose a degradation mechanism. The chemical analysis on the surface and bulk of the films indicates the formation of cesium oxide after UV exposure, with no significant change in the crystalline structure. The proposed mechanism explains the formation of cesium oxides during UV exposure. The *I*−*V* characteristics of diode structures also showed significant degradation after UV exposure, primarily at lower diode rectification ratios. The mechanism proposed in this paper can contribute to developing strategies to enhance the long-term stability of inorganic lead halide perovskites under UV exposure.

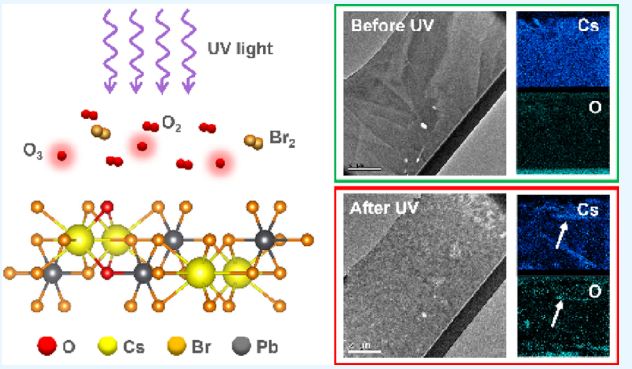

1. INTRODUCTION

Lead halide perovskites ($APbX_3$, where A can be MA^+, FA^+ or Cs^+ and X can be Cl^-, Br^- or I^-) have several advantages, including relatively simple synthesis, tunable band gap, high mobility−lifetime product ($\mu\tau$), and, very important for radiation detection, high average atomic number. Because of these exceptional optoelectronic properties, several applications have been explored, including photodetectors, photovoltaics (PVs), and high-energy radiation detection.[1] Some issues that still need to be solved include environmental concerns related to lead and long-term stability, with the latter being the most critical factor.

Photovoltaic (PV) devices typically operate under aggressive conditions. The use of perovskite materials in solar cells will likely accelerate material degradation due to the aggressive conditions of temperature, moisture, oxygen, and UV light exposure. Recently, moisture has been identified as a primary cause of degradation in hybrid lead halide perovskites.[1] For $MAPbI_{3-x}Cl_x$ and $MAPbI_3$, exposure to moisture leads to the sublimation of MA^+ groups and subsequent decomposition into PbI_2.[1] The hydrophilic nature of lead halide perovskites further accelerates this process.[2] Moisture not only induces decomposition but also accelerates ion migration and phase transformation. Dastidar et al. reported a rapid $\alpha \rightarrow \delta$-phase transformation in bulk $CsPbI_3$ thin films under ambient conditions with relative humidity as low as 11%. At the same time, a control sample stored in a dry N_2 atmosphere exhibited good α-phase stability.[3]

Other factors, such as oxygen and visible light, also impact the degradation of hybrid lead halide perovskites. Senocrate et al. demonstrated that irradiation of $MAPbI_3$ with a Xe-arc lamp changes oxygen molecules into superoxide species (O_2^-). This superoxide species subsequently triggers the deprotonation of MA^+ and the oxidation of iodide.[4] Reactive oxygen species, such as superoxide O_2^- and hydroxide radicals (·OH), have

Received: April 17, 2024
Revised: May 14, 2024
Accepted: May 27, 2024
Published: June 3, 2024

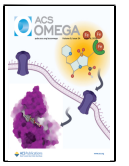

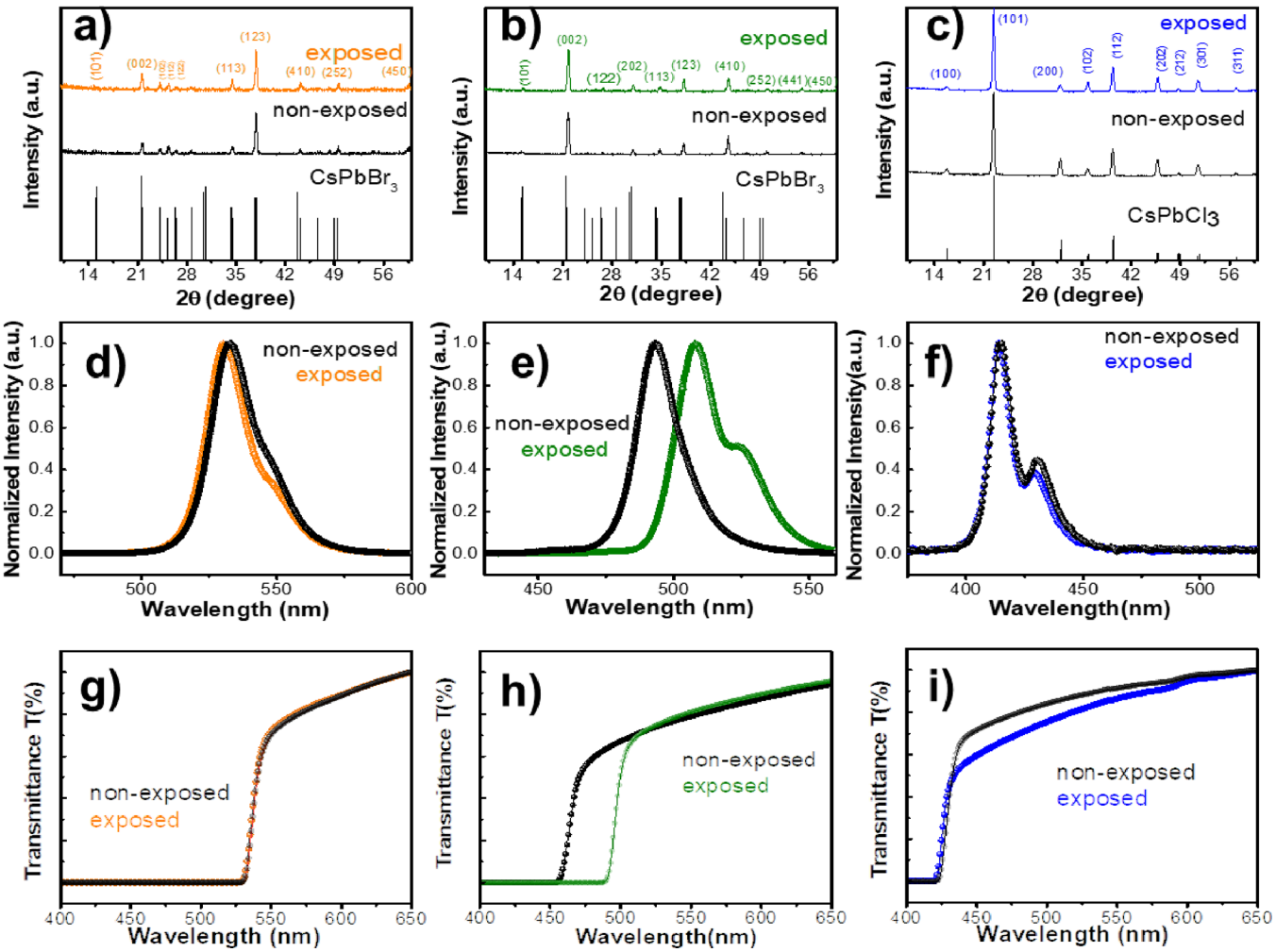

Figure 1. XRD patterns of nonexposed thin films and (a) $CsPbBr_3$, (b) $CsPbBr_2Cl$, and (c) $CsPbCl_3$ exposed to UV for 10 days. Photoluminescence (PL) results of nonexposed and 10 day UV-exposed thin films of (d) $CsPbBr_3$, (e) $CsPbBr_2Cl$, and (f) $CsPbCl_3$. UV−vis results of nonexposed and 10 day UV-exposed thin films of (g) $CsPbBr_3$, (h) $CsPbBr_2Cl$, and (i) $CsPbCl_3$.

also been identified during the photocatalytic process of $CsPbX_3$, although their role in long-term $CsPbX_3$ stability remains only partly understood.[5]

Current reports for the stability of lead halide perovskites primarily focus on hybrid lead halide perovskites with MA^+ and/or FA^+ cations and I-containing compositions with limited reports for inorganic halide perovskites. It is important to note that, for example, inorganic cesium-based lead halide perovskite with Br and Cl anions exhibits remarkable stability under ambient conditions. For instance, orthorhombic $CsPbBr_3$ devices demonstrated exceptional stability when exposed for 3 months to high humidity and room temperature.[6] However, these studies do not address the impact on performance for $CsPbX_3$ (X = Br or Cl) materials and devices under more severe conditions. Recently, Li et al. reported the formation of a new Cs_4PbBr_6 phase within a $CsPbBr_3$ nanocrystal (NC) thin film after exposing the material to UV irradiation (365 nm) for 10 h. They also report the formation of PbO and $PbCO_3$ upon exposure to UV.[7] Ruan et al. noted that surface stoichiometry influences the degradation of $CsPbBr_3$ NCs under UV irradiation, highlighting the poor photostability for Br-rich surfaces.[8] The stability of $CsPbX_3$ devices under ambient conditions and intense UV light exposure still needs to be investigated appropriately. In this paper, the stability of three halide perovskite compositions, $CsPbBr_3$, $CsPbBr_2Cl$, and $CsPbCl_3$ polycrystalline thin films, is presented, and their phase stability, chemical composition, microstructure, and optical properties after exposure to deep-UV radiation in ambient conditions are discussed. To better understand the impact of the perovskite degradation on device performance, ITO/Ga_2O_3/$CsPbX_3$/Au vertical structure diode devices were tested *in situ* under the same UV irradiation conditions. The results in this paper reveal that an amorphous phase of cesium oxide forms during UV exposure without forming a new perovskite phase or significantly affecting the optical properties. However, the electrical properties of the devices are degraded, as discussed later in this paper.

Moreover, these results indicate that the amount of oxygen incorporated into the thin films after exposure to UV radiation is proportional to the chlorine content in the as-deposited films. This oxide formation process further contributes to the degradation of the *I*−*V* performance in the diodes after exposure to UV. Finally, a mechanism based on ion migration is proposed to explain cesium oxide formation.

2. RESULTS

To better study the impact of UV exposure on $CsPbBr_3$, $CsPbBr_2Cl$, and $CsPbCl_3$, a control set of samples (unexposed)

https://doi.org/10.1021/acsomega.4c01461
ACS Omega 2024, 9, 26683−26691

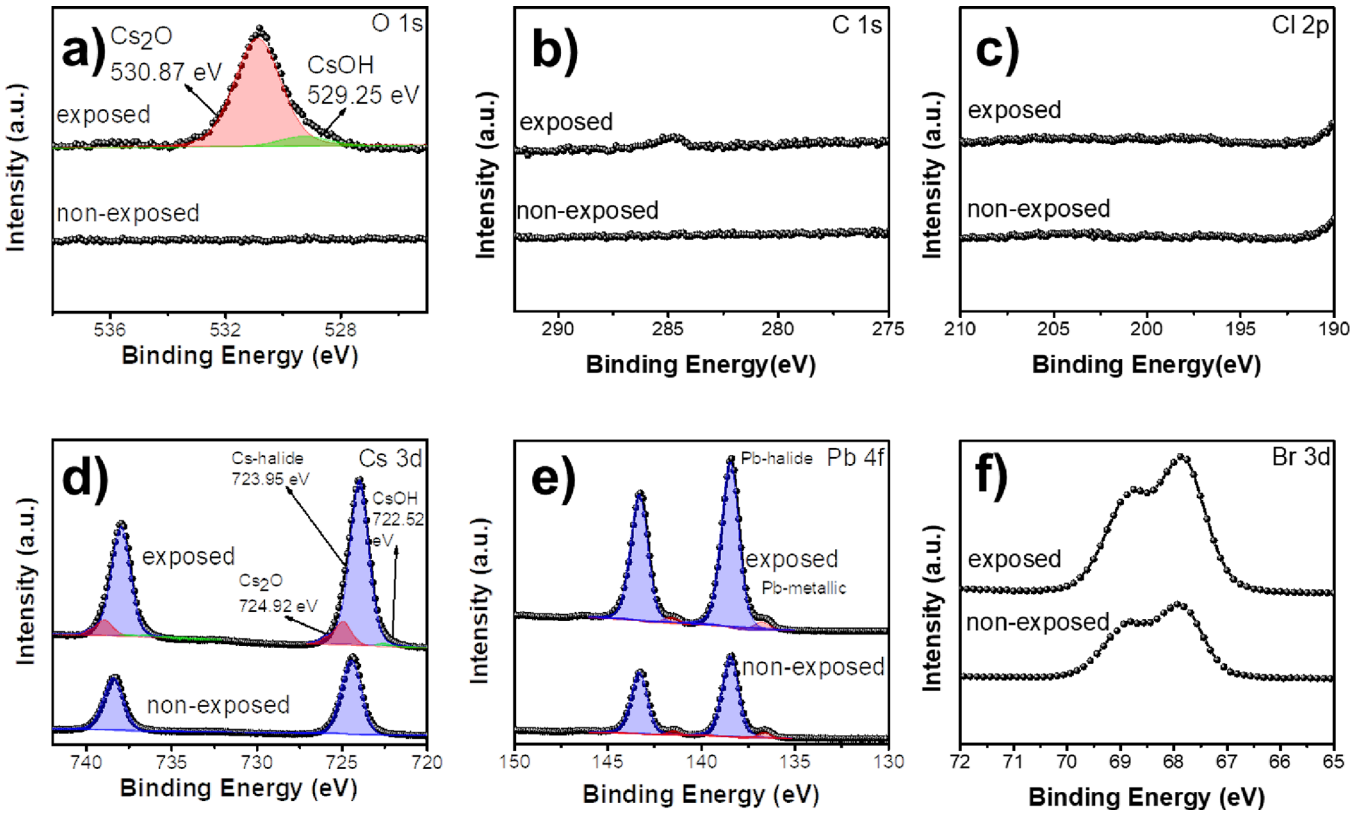

Figure 2. (a) O 1s, (b) C 1s, (c) Cl 2p, (d) Cs 3d, (e) Pb 4f, and (f) Br 3d XPS spectra of nonexposed and 10 day UV-exposed $CsPbBr_3$ thin film.

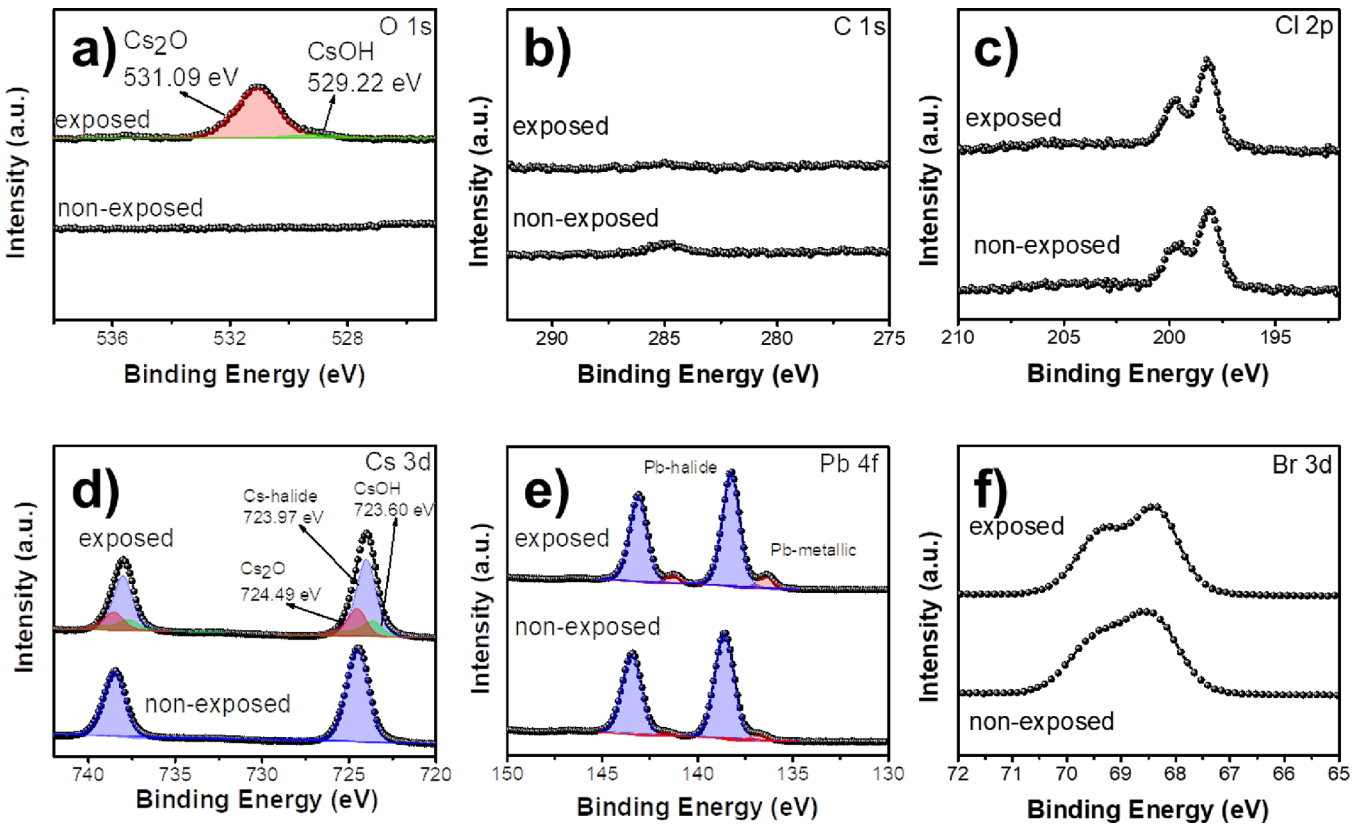

Figure 3. (a) O 1s, (b) C 1s, (c) Cl 2p, (d) Cs 3d, (e) Pb 4f, and (f) Br 3d XPS spectra of nonexposed and 10 day UV-exposed $CsPbBr_2Cl$ thin film.

https://doi.org/10.1021/acsomega.4c01461
ACS Omega 2024, 9, 26683−26691

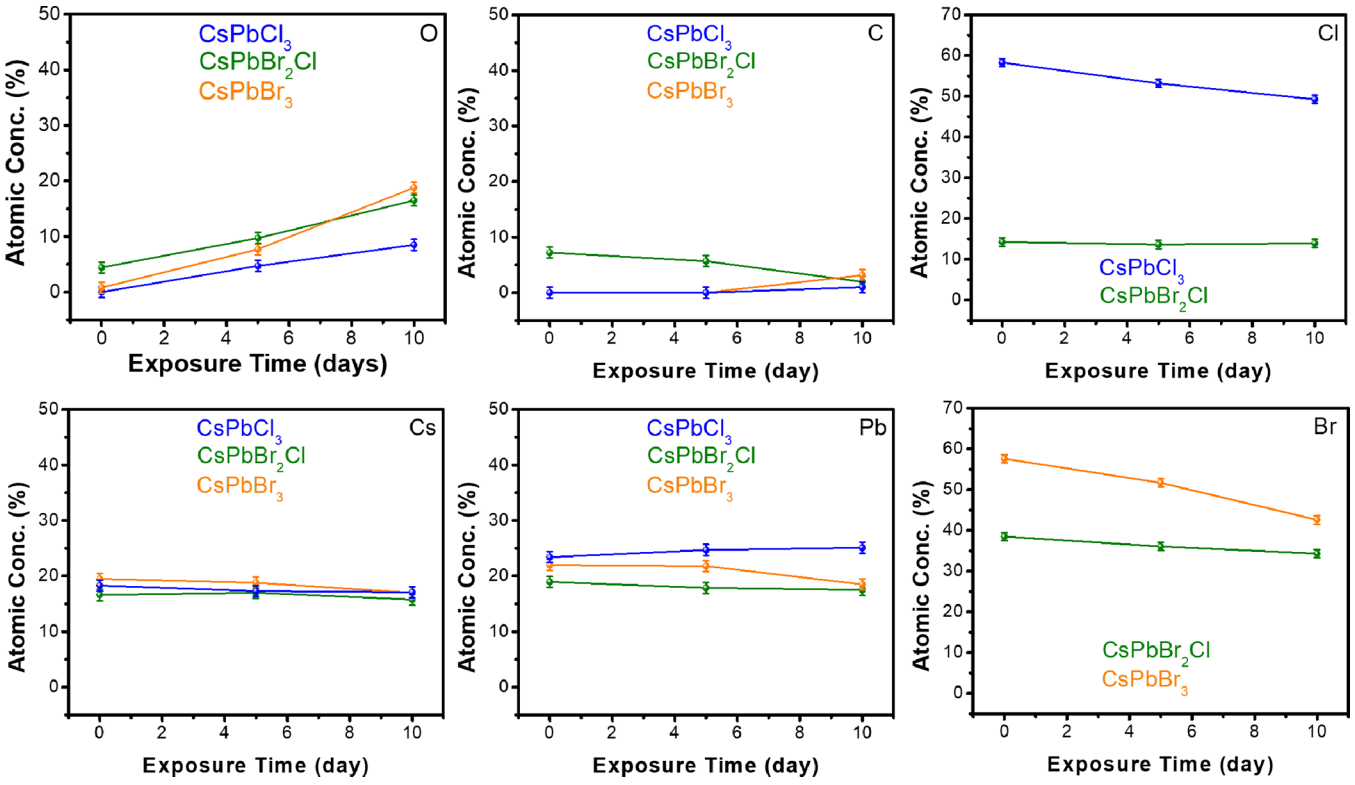

Figure 4. Atomic concentration after UV exposure was calculated from the XPS data for $CsPbBr_3$ (orange), $CsPbBr_2Cl$ (olive), and $CsPbCl_3$ (blue).

was used. The control samples underwent the same preparation and device fabrication conditions as the UV-exposed samples except for UV irradiation. In this paper, the control samples are called "nonexposed". The normalized X-ray diffraction (XRD), photoluminescence (PL), and UV−vis data for nonexposed and UV-exposed films for 10 days are shown in Figure 1a−c. The nonexposed films were stored under ambient conditions for 10 days and measured at the same time as the films exposed to UV radiation. The XRD results did not show significant changes after exposure in any of the compositions investigated in this work. In Figure 1b, the XRD pattern of $CsPbBr_2Cl$ has a small shift compared with the standard $CsPbBr_3$ pattern, indicating a slight change of the lattice constant. A detailed discussion regarding this effect can be found in a previous publication from our group.[9] Figure 1d−f and g−i show the PL and UV−vis spectra results for nonexposed and exposed $CsPbBr_3$, $CsPbBr_2Cl$, and $CsPbCl_3$ films, respectively. The PL spectra for $CsPbBr_3$ show two emission peaks with a separation of 10 nm centered at around 530 nm with no significant change after exposure.

On the other hand, the PL for exposed $CsPbBr_2Cl$ shows a substantial change in the shape of the emission band and a clear redshift. A detailed analysis and explanation of this phenomenon are given in Section 3. The UV−vis results show that there is a redshift for the absorption edge of the $CsPbBr_2Cl$ sample after UV exposure, which correlated to what was found in PL results, and also, the transmission rate of $CsPbCl_3$ decreased below the absorption edge after exposure; this change is due to metallic lead formation after UV exposure. However, the absorption edge of the perovskites remains the same. It is essential to mention that the nonexposed and "as-deposited" perovskites did not show any change. Hence, the experimental data corresponding to "as-deposited" are omitted in the discussion, but the results can be found in Figure S1.

Figure 2 shows the X-ray photoelectron spectroscopy (XPS) results for nonexposed and exposed $CsPbBr_3$ films. The O 1s region in Figure 2a shows a new band around 532 eV after UV exposure. The deconvolution of this band indicates that the O 1s is formed by two contributions at 530.87 and 529.25 eV corresponding to Cs_2O and CsOH, respectively.[10] This is consistent with the analysis of the Cs 3d region shown in Figure 2d, where there are two new contributions after UV exposure at 724.92 and 722.52 eV corresponding to Cs_2O and CsOH, respectively.[10] Notably, no oxidized species are observed within the detection limit of XPS in the Pb 4f spectra. A small trace of carbon was still present in the exposed sample, which can be attributed to the remaining carbon contamination from the cleaning process. These results strongly suggest that oxygen is mostly bonded to cesium. The metallic lead band observed in the Pb 4f spectra results from the cleaning procedure using argon ions (Ar^+) to sputter-clean the surface before the XPS analysis.[11] Although Ar^+ cleaning can modify the surface composition, the sputtering time was kept at a minimum to remove the surface contamination, whereas no other undesired effects were induced.

The XPS data of nonexposed and 10 day UV-exposed $CsPbBr_2Cl$ films are shown in Figure 3. Like $CsPbBr_3$, Cs_2O and CsOH peaks are observed in the O 1s and Cs 3d spectra. For detailed peak fitting parameters used for Figures 2 and 3, please see Tables S1 and S2.

Figure 4 shows the elemental compositions obtained by XPS for $CsPbBr_3$, $CsPbBr_2Cl$, and $CsPbCl_3$ during UV exposure. The atomic concentration of oxygen is proportional to the exposure time: the longer the exposure is, the more oxygen is

https://doi.org/10.1021/acsomega.4c01461
ACS Omega 2024, 9, 26683−26691

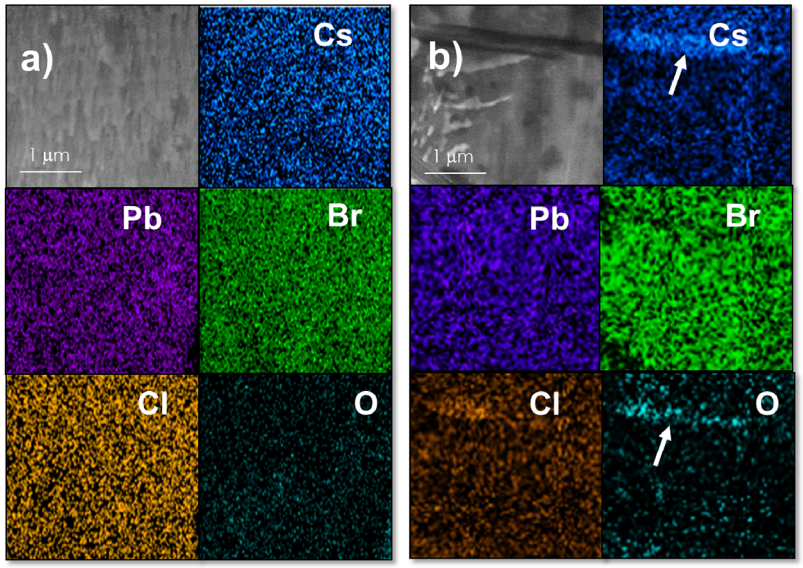

Figure 5. TEM and EDX mapping of (a) nonexposed and (b) 10 day UV-exposed $CsPbBr_2Cl$ thin films. The white arrow indicates high-concentration regions for Cs and O.

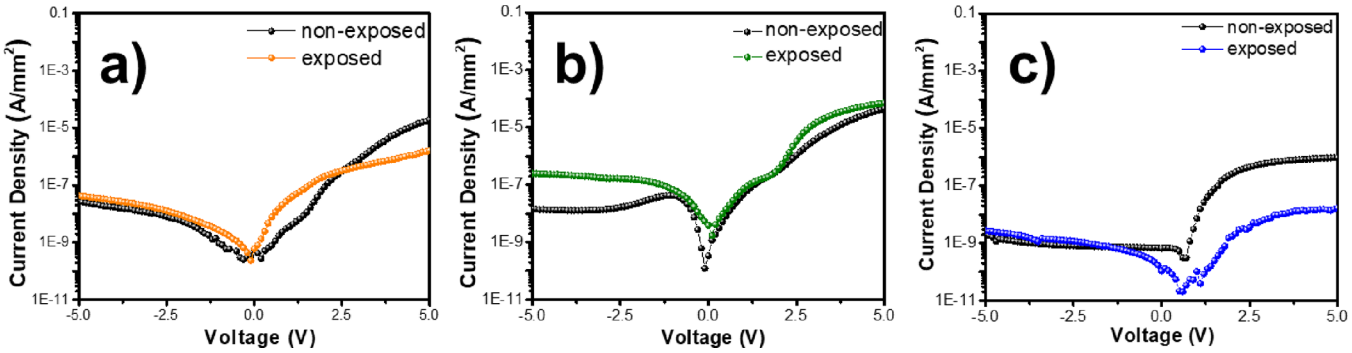

Figure 6. *I*−*V* measurement results of nonexposed and 10 day UV-exposed (a) $CsPbBr_3$, (b) $CsPbBr_2Cl$, and (c) $CsPbCl_3$ thin film-based diodes.

incorporated into the material. A small decrease in the halide concentration also indicates a correlation between cesium oxide formation and halide reduction. XPS results for the three compositions for shorter UV exposure time are shown in the Supporting Information (Figure S3). Among all of the compositions studied, $CsPbBr_2Cl$ has the fastest rate of oxide formation during UV exposure. The mechanism proposed in Section 3 further discusses this phenomenon.

Transmission electron microscopy (TEM) and energy-dispersive X-ray spectroscopy (EDS) studies were conducted on exposed and nonexposed perovskite films to investigate further the effects of UV exposure on the perovskite films. The samples were prepared using standard focused ion beam (FIB) protocols and then observed using TEM (Figure S5a−c). Large grains were observed, and the crystalline structure was confirmed by using the selected-area electron diffraction pattern (SADP, Figure S6). Cross-section TEM images and EDS maps for nonexposed and exposed $CsPbBr_2Cl$ are shown in Figure 5. The contrast difference in the images for exposed (Figure 5b) and nonexposed (Figure 5a) films suggests a change in the grain size or structure of the perovskite. This change was confirmed with electron-diffraction data (Figure S6).

EDS elemental maps of selected areas were acquired to evaluate the elemental distribution. EDS maps display a homogeneous distribution of elements for nonexposed films. In contrast, EDS maps of the sample exposed to UV reveal regions with higher concentrations of cesium and oxygen, which are direct evidence of cesium oxide formation. Some other changes, including elemental segregation, were observed in some regions in exposed films, suggesting the formation of secondary phases (Figure 5b, arrow-pointed region). The film exposed to UV radiation (Figure 5b) shows the most remarkable changes, as observed in the TEM results.

At this point, the hypothesis is that oxygen diffuses into the film along the grain boundaries, as the oxidation is in the bulk of the film and not exclusive to the surface. Also, halide ions diffuse faster along the grain boundaries because of the UV irradiation and oxygen atoms, which then substitute for the halide ions. A detailed explanation of this phenomenon is shown in Section 3.

Vertical diodes were fabricated to investigate the impact of UV exposure on the electrical performance of the resulting devices. And the *I*−*V* characteristics of the diodes measured *in situ* during UV exposure are shown in Figure 6. There is clearly performance degradation in the reverse current for the $CsPbBr_2Cl$ diodes after exposure, increasing by 10×, whereas for $CsPbBr_3$ and $CsPbCl_3$, only the forward current decreases. The degradation in $CsPbBr_2Cl$ is likely attributed to the formation of cesium oxide during UV exposure, leading to

https://doi.org/10.1021/acsomega.4c01461
ACS Omega 2024, 9, 26683−26691

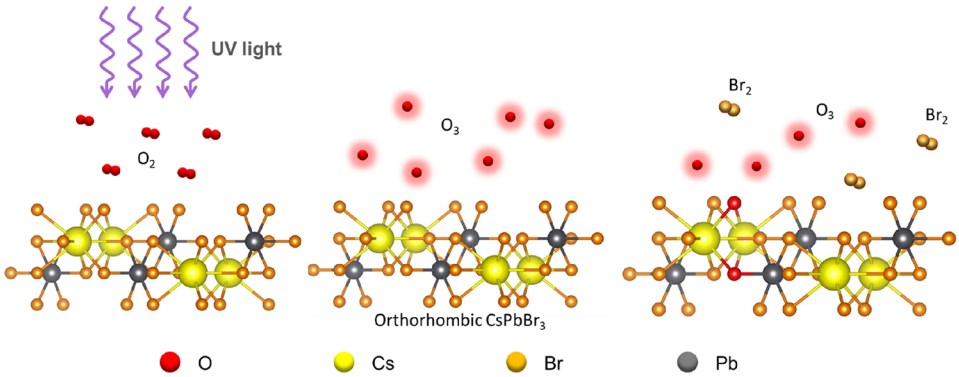

Figure 7. Illustration of the proposed cesium oxide formation process during UV exposure. First, $CsPbX_3$ perovskites are exposed to UV irradiation (left), oxygen molecules are excited, and active oxygen species are generated (shown as O_3), which are shown as glowing red circles. Finally, these active oxygen species react with the surface halide ions, oxidize, and replace them in the perovskite structure. The halide ions turn into halogen molecules and desorb from the surface.

conductive pathways and subsequent deterioration in the diode performance. The different behavior in the *I*−*V* characteristics for the mix-halide ($CsPbBr_2Cl$) and nonmixed halide ($CsPbBr_3$ and $CsPbCl_3$) composition is likely due to the agglomeration of the oxides among the different compositions. Anion phase segregation induced by UV irradiation facilitates the diffusion of oxygen ions into the bulk of the mixed-halide $CsPbBr_2Cl$ thin film, accelerating cesium oxide formation. As for nonmixed halides ($CsPbBr_3$ and $CsPbCl_3$), anion phase segregation does not exist, and oxide formation happens near the surface and not the bulk volume.

3. DISCUSSION

The results presented in the previous section provide sufficient evidence to establish that, after UV exposure, the crystalline structures remain nearly unchanged, the electrical properties of vertical diode structures deteriorate, and there is the formation and likely segregation of CsOx. This allows us to propose a mechanism for forming oxidized species of cesium and how it impacts device performance. Several reports have shown ion migration as a common phenomenon in lead halide perovskite materials normally induced by an electric field or irradiation. The main migration species are the halogen ions.[12−15] First-principles density functional theory (DFT) analysis by Biega et al. found that the energy barrier for ion migration of bromide ion (Br^-) is significantly lower on the surface and subsurface compared to the bulk.[16] In other words, bromide ions are more prone to migrate when closer to the surface, turning the surface into a Br-rich region. As bromide ions migrate to the surface, they create a negatively charged environment, attracting cesium ions (Cs^+) moving toward the surface due to the Coulombic forces.

The low-pressure mercury lamp used in this paper has its main emission in the deep-UV region (255 nm). This UV radiation has enough energy to excite oxygen molecules and generate active oxygen species such as O_2^-, ozone, and hydroxide radical ·OH. When inorganic lead halide perovskites are exposed to these active oxygen species, halide ions (Br^- and Cl^- in this case) undergo oxidation, forming molecular Br_2 and Cl_2 halogens that subsequently leave the surface. Sjostedt et al. also reported similar gas-phase halogens released from metallic halide solid surfaces.[17] The proposed model in our work considers that newly formed O_{Br} (oxygen occupying Br sites in the lattice) diffuses into the perovskite, forming oxidized cesium species.

The XPS results show that $CsPbBr_3$ has no oxidation after 24 h UV exposure (see Figure S3). In contrast, $CsPbBr_2Cl$ shows oxide formation after just 8 h of UV exposure, and as for $CsPbCl_3$, oxides are formed after 18 h of exposure. It is crucial to highlight that the mixed halide $CsPbBr_2Cl$ perovskite exhibits the fastest oxidation rate. This can be explained by light-induced anion phase segregation. As summarized by Brennan et al., for $CsPbX_3$, halide ion vacancies have smaller formation energy than Cs^+ and Pb^{2+} vacancies, resulting in high mobility for halide ions in $CsPbX_3$ perovskites.[18] It has also been reported that mixed lead halide perovskites, such as $MAPb(I_{3-x}Br_x)$, show a phase segregation behavior, forming I- and Br-rich domains separately when exposed to continuous visible light irradiation.[18] A similar process happens when a mixed inorganic halide perovskite ($CsPbBr_2Cl$) is exposed to UV light, forming Br-rich and Cl-rich domains. Figure 1e,h shows that the redshift and presence of new peaks correspond to the formation of more Br-rich and $CsPbBr_3$ phases, thus showing anion phase segregation. Even if the concentration of the latter is below 1%, it can still have an impact on the PL spectra and electrical properties, although it may not be detectable by XPS or XRD. This anion phase segregation process facilitates the absorption and diffusion of oxygen atoms in $CsPbBrCl_2$ during UV exposure in ambient conditions compared to nonmixed halides ($CsPbBr_3$ and $CsPbCl_3$). Thus, oxide formation is faster in $CsPbBr_2Cl$ than in non halide-mixed perovskite compositions. Anion phase segregation not only affects the accumulation rate of oxide in the films but also impacts the electrical measurement results of exposed diode devices; note that, in Figure 6, the forward current of exposed $CsPbBr_3$ and $CsPbCl_3$ decreased, whereas exposed $CsPbBr_2Cl$ remained almost identical. This difference can be explained by the fact that because of the anion phase segregation that happened in $CsPbBr_2Cl$, oxygen species can infiltrate and disperse in the whole bulk of $CsPbBr_2Cl$, whereas for $CsPbBr_3$ and $CsPbCl_3$, formed oxides can only accumulate on the surface of perovskite thin film because of the vertical structure configuration of the diode. This region directly contacts the Au electrode; thus, accumulated oxides deteriorate the interface properties between perovskite and Au.

The energy for orthorhombic $CsPbBr_3$ to decompose into CsBr and $PbBr_2$ is 0.3 eV, whereas for orthorhombic $CsPbCl_3$ to decompose into its two binary precursor compounds, the energy is 0.08 eV.[19] This suggests that $CsPbCl_3$ is more likely to decompose than $CsPbBr_3$. In other words, $CsPbCl_3$

https://doi.org/10.1021/acsomega.4c01461
ACS Omega 2024, 9, 26683−26691

generates more defects and vacancies under UV light, increasing the ion migration process. Consequently, more halide ions migrate to the surface, leading to increased oxidation. An illustration of the proposed mechanism is depicted in Figure 7.

4. CONCLUSIONS

This work investigated the stability of polycrystalline cesium-based lead halide perovskites $CsPbBr_3$, $CsPbBr_2Cl$, and $CsPbCl_3$ thin films under extended exposure to deep-UV radiation. It is shown that, after exposure, the crystalline structure remains unchanged, but oxidized species of cesium are formed throughout the film, resulting in degraded electrical characteristics of the investigated diode structures. We propose a degradation mechanism that involves active oxygen species generated during UV exposure that diffuse into the films through the grain boundary and oxidize and halide ions, forming CsO_x. Furthermore, anion phase segregation induced by UV irradiation facilitates the infiltration and diffusion of oxygen ions into the bulk of the mixed-halide $CsPbBr_2Cl$ thin film. This will transport oxygen ions throughout the thin film, accelerating the exchange of oxygen ions and halide ions. As halide ions are replaced by oxygen, cesium oxides are formed. As for nonmixed halides ($CsPbBr_3$ and $CsPbCl_3$), anion phase segregation does not exist, so the oxide formation can happen mainly near the surface and not the bulk of the film. Thus, the mixed halide perovskite sample shows the fastest oxide formation rate. This study emphasizes the correlation between the amount of incorporated oxygen and the chlorine content in the perovskite films, with $CsPbBr_2Cl$ exhibiting the fastest rate of oxide formation. These results highlight the need for better strategies to enhance the long-term stability of inorganic perovskites, particularly when they are used in harsh conditions.

5. EXPERIMENTAL SECTION

Materials. Lead(II) bromide (99.999%), lead(II) chloride (98%), cesium bromide (99.9%), and cesium chloride (99.9%) were purchased from Sigma-Aldrich.

Powder Precursor Synthesis for Close Space Sublimation (CSS). Two compositions of CSS powder precursors, $CsPbBr_3$ and $CsPbCl_3$, were synthesized by a ball-milling process using an MSE PRO benchtop mini high-energy vertical planetary ball mill system. Each precursor's stoichiometric molar amounts (2.5 mmol of each CsX and PbX_2) were weighed and placed inside a stainless-steel jar. Additionally, milling balls with 5× the weight of the precursors were added to the jar to carry out the reaction and help to grind and unify the product into a micrometer size. Subsequently, the stainless-steel jar was placed inside the planetary ball-milling system, and the optimum parameters were set for the synthesis. The rotating speed was set to 700 rpm, with a total milling time of 12 h and forwarding and reverse times of 20 min each. The intervals between forwarding and reversing are set at 10 min each. Finally, after 12 h, the perovskite powders were collected from the jar, placed into the vial, sealed with parafilm, and kept in the glovebox to avoid contamination until needed for the CSS process.

CSS Deposition of Films. The deposition of the $CsPbBr_3$ films was carried out under a vacuum (70 mTorr). The temperatures of the source and substrate (1 × 1 $in.^2$ glass) in the CSS process were set at 500 and 200 °C, respectively. The distance between the powder precursor source and the substrate was 5 mm. The deposition of the $CsPbCl_3$ films was carried out under the same vacuum as $CsPbBr_3$ films, but the source and substrate temperatures in the CSS process were set at 550 and 275 °C, respectively. The thickness of the film was controlled by varying the deposition time. For details of the CSS process, please check the previous publication from our group.[20]

$PbCl_2$ Thermal Treatment Process. $CsPbBr_3$ films were annealed immediately after deposition in the same CSS system using $PbCl_2$ salts as the halogen source. During the vapor treatment, the source and substrate temperatures were maintained at 400 and 425 °C, respectively. The higher substrate temperature eliminates any deposition of a $PbCl_2$ layer over the perovskite film. The extent of ion exchange was controlled by the annealing time. The film's color change after the thermal processing shows evidence of ion exchange. For the details of this ion exchange process, please refer to the previous publication from our group.[9]

Device Fabrication. The pn diodes with the ITO/Ga_2O_3/perovskite/Au structure were fabricated using Ga_2O_3 as the n-type semiconductor and deposited on a patterned (photolithography) ITO/glass (thickness ≈140 nm) substrate that serves as the bottom contact. Approximately 120 nm of Ga_2O_3 was deposited by RF sputtering from a Ga_2O_3 target acquired from Kurt J. Lesker Company. The deposition was conducted at room temperature using a sputter power density of 17.83 W cm^{-2} under a 100% Ar ambient atmosphere and a total pressure of 3 mTorr. Before deposition, all substrates were cleaned in an ultrasonic bath using acetone, 2-propanol, and deionized water in that order and dried with N_2 gas. A photolithographic process defined the size of the ITO and Ga_2O_3 layers and the diode diameters (250 μm, 500 μm, 1 mm, and 2 mm). The perovskite films ($CsPbBr_3$, $CsPbCl_3$, or $CsPbBr_2Cl$) (∼8 μm) were deposited by CSS on top of ITO/Ga_2O_3 as described above. Finally, the top contact, 200 nm thick Au, was deposited through a shadow mask in an e-beam evaporator at a rate of 0.1 Å/s.

Characterization of the Film and Diode. The $I-V$ characteristics were measured. The resulting diodes were measured using a probe station (Cascade SUMMIT 11741B-H) equipped with a Keithley 4200 and HP 4280A. UV−vis measurements were carried out to estimate the Eg from the transmittance spectra of the $CsPbX_3$ films using an Agilent Technologies Cary 5000 UV−vis-NIR double beam spectrophotometer with a mercury lamp as the light source; the scan range was 300−800 nm.

The crystalline structure of the films was determined using GIXRD (Rigaku SmartLab X-ray diffractometer) using a Cu Kα X-ray source at grazing incident angles of 0.5 and 2.0°. The XPS measurements were performed using a PHI 5000 Versa Probe II. All the data were taken at a 45° takeoff angle with respect to the sample surface. A monochromatic Al Kα radiation source ($h\nu$ = 1486.6 eV) with a 0.125 eV step size and a pass energy of 29.35 eV was used. The base pressure in the analysis chamber was better than 1.0×10^{-9} Torr. The sample surfaces were cleaned using Ar^+ from a FIG5 ion gun at 2 kV and an area of 3 × 3 mm for 30 s. All binding energies reported in this work are relative to the C 1s peak at 284.8 eV. PL was recorded using an in-house-built system with neutral density filters.

UV Exposure Experiment. The exposure experiment was conducted under ambient conditions in a dark box with a

https://doi.org/10.1021/acsomega.4c01461
ACS Omega 2024, 9, 26683−26691

relative humidity of 40−50%. The UV light source was a UVGL-25 tube lamp purchased from UVP. The irradiation power received by samples was calibrated with a ThorLabs S120VC Si photodetector to be 4 mW and monitored throughout the exposure session. *In situ* $I-V$ measurements of devices were taken using a Keithley 2400 sourcemeter; UV light was turned off when conducting $I-V$ measurements. The sweep range was from −10 to 10 V with a step size of 0.1 V. Multiple sweeps (at least five5 times) were taken to rule out outlier data sets and confirm steady-state behavior.

TEM and FIB Experiments. Exposed and nonexposed $CsPbBr_{3-x}Cl_x$ films were characterized using TEM and EDS. Cross-section specimens were prepared using an FIB system with a gallium ion source (FEI-ThermoFisher Nova 200 FIB/SEM) and mounted on a copper mesh for TEM analysis. FIB-TEM lamellae were observed using a JEOL ARM200F operated at an accelerating voltage of 200 kV. EDS maps were acquired using an Oxford X-Max EDS instrument with the Aztec Software.

■ ASSOCIATED CONTENT

Supporting Information

The Supporting Information is available free of charge at https://pubs.acs.org/doi/10.1021/acsomega.4c01461.

XPS spectra of as-deposited $CsPbBr_3$ thin films, nonexposed and 10 day UV-exposed $CsPbCl_3$ thin films, and short-term UV-exposed $CsPbX_3$ thin films; cross-section TEM image and SADP of nonexposed and 10 day UV-exposed $CsPbX_3$ thin films; time-resolved PL of nonexposed and 10 day UV-exposed $CsPbBr_3$ thin films; XPS spectra of 10 day UV-exposed $CsPbBr_3$ sample under a controlled glovebox environment; and XPS peak fitting parameters (PDF)

■ AUTHOR INFORMATION

Corresponding Author

Manuel A. Quevedo-Lopez − *Department of Material Science and Engineering, The University of Texas at Dallas, Richardson, Texas 75080, United States;* orcid.org/0000-0002-1867-7584; Email: mquevedo@utdallas.edu

Authors

Zhiyang Qin − *Department of Material Science and Engineering, The University of Texas at Dallas, Richardson, Texas 75080, United States*

Jesus Alfonso Caraveo-Frescas − *Department of Material Science and Engineering, The University of Texas at Dallas, Richardson, Texas 75080, United States;* orcid.org/0000-0002-5386-7762

Leunam Fernandez-Izquierdo − *Department of Material Science and Engineering, The University of Texas at Dallas, Richardson, Texas 75080, United States*

M. Josefina Arellano-Jimenez − *Department of Material Science and Engineering, The University of Texas at Dallas, Richardson, Texas 75080, United States*

Francisco S. Aguirre-Tostado − *Department of Material Science and Engineering, The University of Texas at Dallas, Richardson, Texas 75080, United States; Centro de Investigacion en Materiales Avanzados, Apodaca, NL 66628, Mexico;* orcid.org/0000-0002-8721-0179

Martin Gregorio Reyes-Banda − *Department of Material Science and Engineering, The University of Texas at Dallas, Richardson, Texas 75080, United States;* orcid.org/0000-0002-5077-0885

Complete contact information is available at: https://pubs.acs.org/10.1021/acsomega.4c01461

Author Contributions

Z.Q., L.F.-I., M.J.A.-J., M.R.-B., and J.A.C.-F. jointly completed the experimental plan, experiments, data analysis, and manuscript writing. Z.Q., L.F.-I., and J.A.C.-F. participated in related discussions and aided the experiments. F.S.A.-T. assisted with manuscript revision and discussion. This project was completed under the guidance and supervision of M.A.Q.-L. All authors have approved the final version of the manuscript.

Notes

The authors declare no competing financial interest.

■ ACKNOWLEDGMENTS

The authors would like to thank The University of Texas at Dallas, Richardson, TX, USA; the cleanroom staff; Zeshaan Shamsi and Monét Royan for sample preparation; Conor Ryan for PL measurement; and Yaoqiao Hu for the discussion about the oxide formation mechanism.

■ REFERENCES

(1) Philippe, B.; et al. Chemical and electronic structure characterization of lead halide perovskites and stability behavior under different exposures-A photoelectron spectroscopy investigation. *Chem. Mater.* **2015**, *27* (5), 1720−1731.

(2) Christians, J. A.; Miranda Herrera, P. A.; Kamat, P. V. Transformation of the excited state and photovoltaic efficiency of CH3NH3PbI3 perovskite upon controlled exposure to humidified air. *J. Am. Chem. Soc.* **2015**, *137* (4), 1530−1538.

(3) Dastidar, S.; et al. High Chloride Doping Levels Stabilize the Perovskite Phase of Cesium Lead Iodide. *Nano Lett.* **2016**, *16* (6), 3563−3570.

(4) Senocrate, A.; et al. Interaction of oxygen with halide perovskites. *J. Mater. Chem. A Mater.* **2018**, *6* (23), 10847−10855.

(5) Gao, G.; et al. Novel inorganic perovskite quantum dots for photocatalysis. *Nanoscale* **2017**, *9* (33), 12032−12038.

(6) Liang, J.; et al. All-Inorganic Perovskite Solar Cells. *J. Am. Chem. Soc.* **2016**, *138* (49), 15829−15832.

(7) Li, J.; et al. Ultraviolet light induced degradation of luminescence in CsPbBr3 perovskite nanocrystals. *Mater. Res. Bull.* **2018**, *102*, 86−91.

(8) Ruan, L. J.; Tang, B.; Shu, A.; Qin, C.; Ma, Y. Self-Passivation of CsPbBr3Nanocrystals through Introducing Bromide Vacancies and Ultraviolet Irradiation. *J. Phys. Chem. C* **2021**, *125* (1), 1010−1017.

(9) Reyes-Banda, M. G.; Fernandez-Izquierdo, L.; Nandagopala Krishnan, S. S.; Caraveo-Frescas, J. A.; Mathew, X.; Quevedo-López, M. Material Properties Modulation in Inorganic Perovskite Films via Solution-Free Solid-State Reactions. *ACS Appl. Electron Mater.* **2021**, *3* (3), 1468−1476.

(10) Ebbinghaus, G.; Simon, A. Electronics structures of Rb, Cs and some of their metallic oxides studied by photoelectron spectroscopy. *Chem. Phys.* **1979**, *43* (1), 117−133.

(11) Busby, Y.; et al. Aging effects in interface-engineered perovskite solar cells with 2D nanomaterials: A depth profile analysis. *Mater. Today Energy* **2018**, *9*, 1−10.

(12) Mosconi, E.; De Angelis, F. Mobile Ions in Organohalide Perovskites: Interplay of Electronic Structure and Dynamics. *ACS Energy Lett.* **2016**, *1* (1), 182−188, DOI: 10.1021/acsenergylett.6b00108.

(13) Meloni, S.; et al. Ionic polarization-induced current-voltage hysteresis in CH3NH3PbX3 perovskite solar cells. *Nat. Commun.* **2016**, *7*, 10334 DOI: 10.1038/ncomms10334.

(14) Luo, Y.; et al. Direct Observation of Halide Migration and its Effect on the Photoluminescence of Methylammonium Lead Bromide Perovskite Single Crystals. *Adv. Mater.* **2017**, *29* (43), 1703451 DOI: 10.1002/adma.201703451.
(15) Senocrate, A.; et al. The Nature of Ion Conduction in Methylammonium Lead Iodide: A Multimethod Approach. *Angew. Chem.* **2017**, *129* (27), 7863−7867.
(16) Biega, R. I.; Leppert, L. Halogen vacancy migration at surfaces of CsPbBr3 perovskites: Insights from density functional theory. *J. Phys. Energy* **2021**, 3 (3), No. 034017, DOI: 10.1088/2515-7655/ac10fe.
(17) Sjostedt, S. J.; Abbatt, J. P. D. Release of gas-phase halogens from sodium halide substrates: Heterogeneous oxidation of frozen solutions and desiccated salts by hydroxyl radicals. *Environ. Res. Lett.* **2008**, 3 (4), No. 045007.
(18) Brennan, M. C.; Draguta, S.; Kamat, P. V.; Kuno, M. Light-Induced Anion Phase Segregation in Mixed Halide Perovskites. *ACS Energy Lett.* **2018**, 3 (1), 204−213.
(19) Evarestov, R. A.; Kotomin, E. A.; Senocrate, A.; Kremer, R. K.; Maier, J. First-principles comparative study of perfect and defective CsPbX3 (X = Br, I) crystals. *Phys. Chem. Chem. Phys.* **2020**, *22* (7), 3914−3920.
(20) Fernandez-Izquierdo, L.; et al. Cesium Lead Bromide (CsPbBr3) Thin-Film-Based Solid-State Neutron Detector Developed by a Solution-Free Sublimation Process. *Adv. Mater. Technol.* **2020**, 5 (12), 2000534.

https://doi.org/10.1021/acsomega.4c01461
ACS Omega 2024, 9, 26683−26691